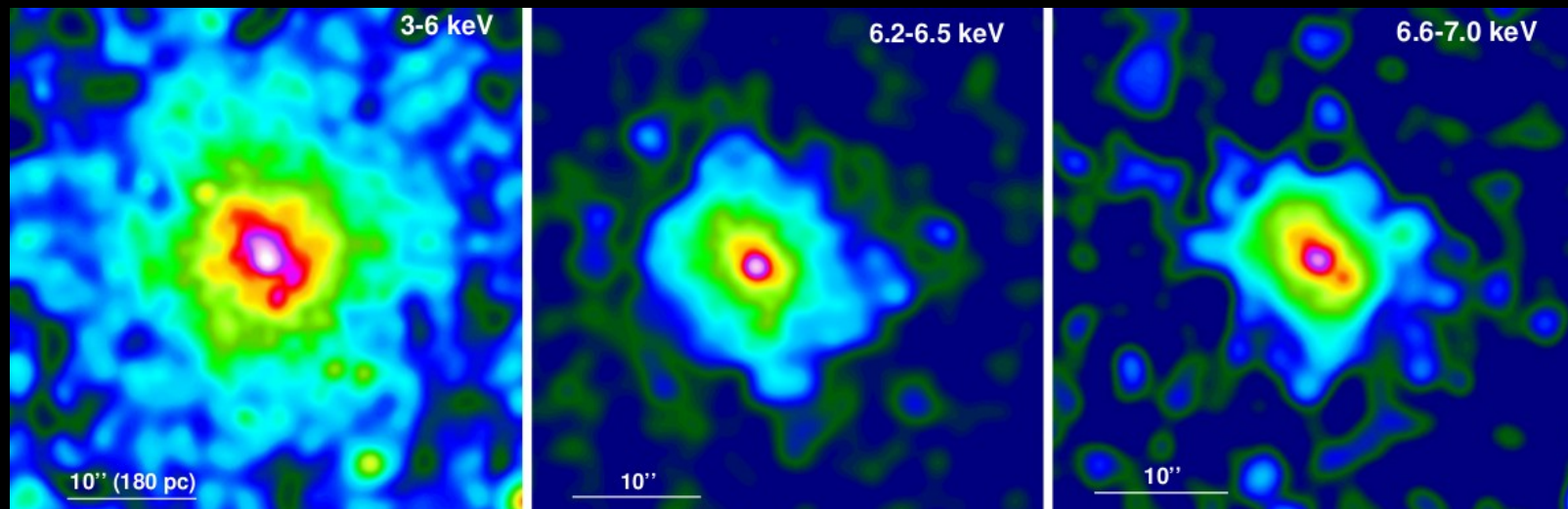


Spatially resolved spectroscopy of NGC 4945



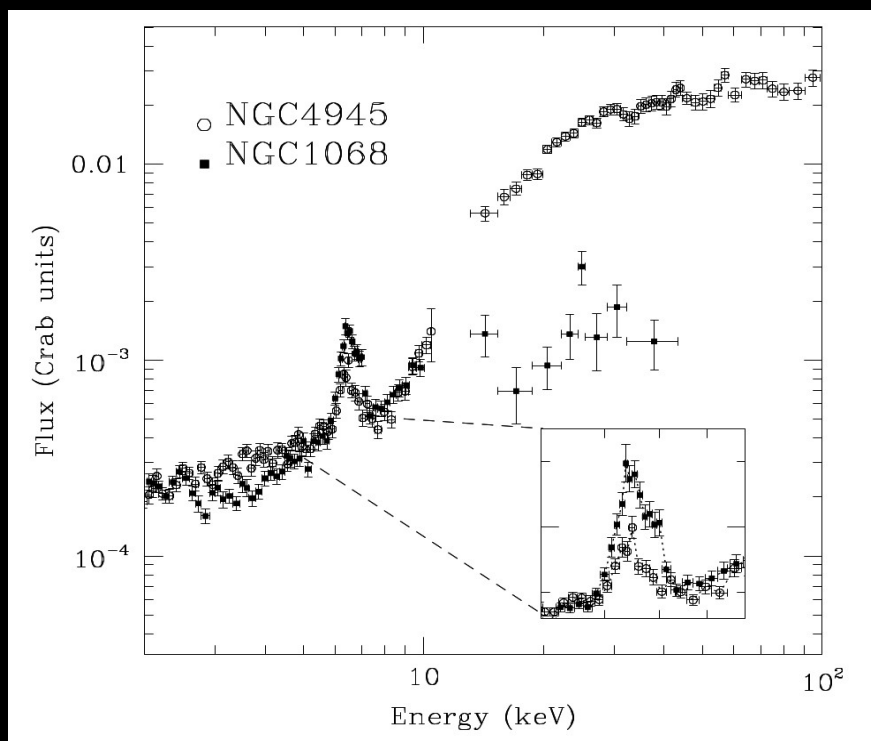
Andrea Marinucci

S. Bianchi, G. Fabbiano, G. Matt, G. Risaliti, E. Nardini, J. Wang



Introduction

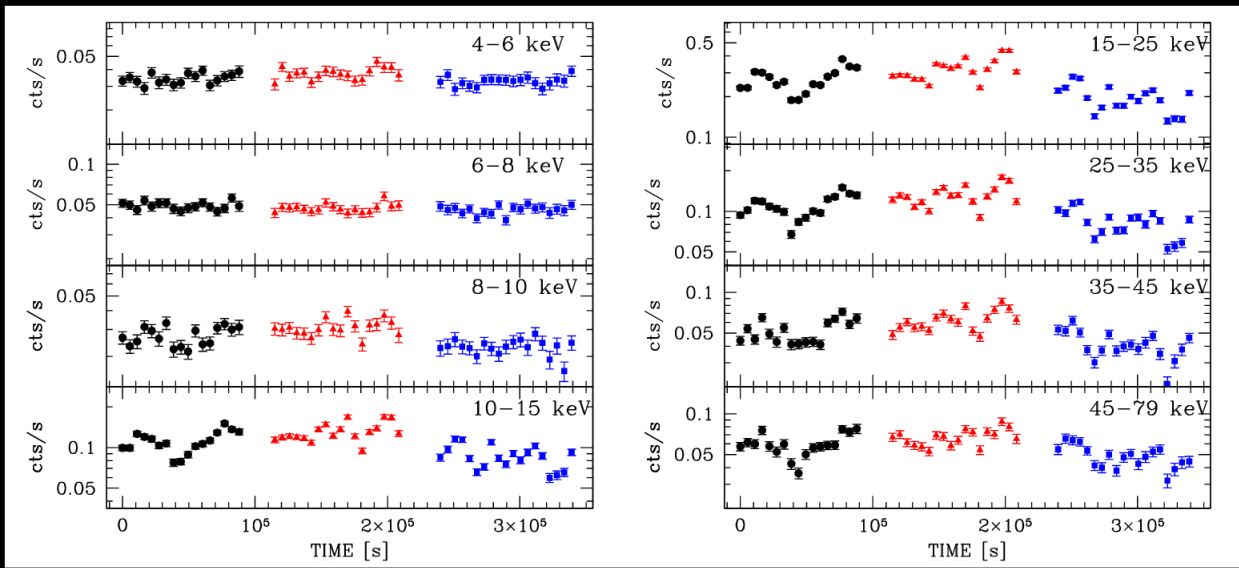
NGC 4945 is a nearby (3.7 Mpc), almost edge-on, spiral galaxy. It is the brightest Sy 2 galaxy and the brightest radio-quiet AGN of the 100 keV sky after NGC 4151 (Done et al, 1996)



Guainazzi+00

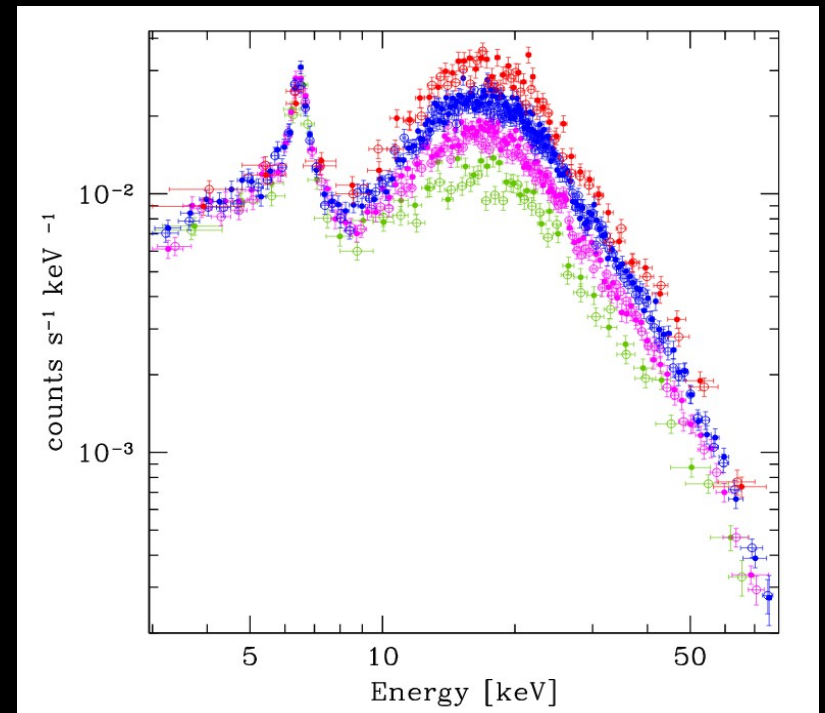
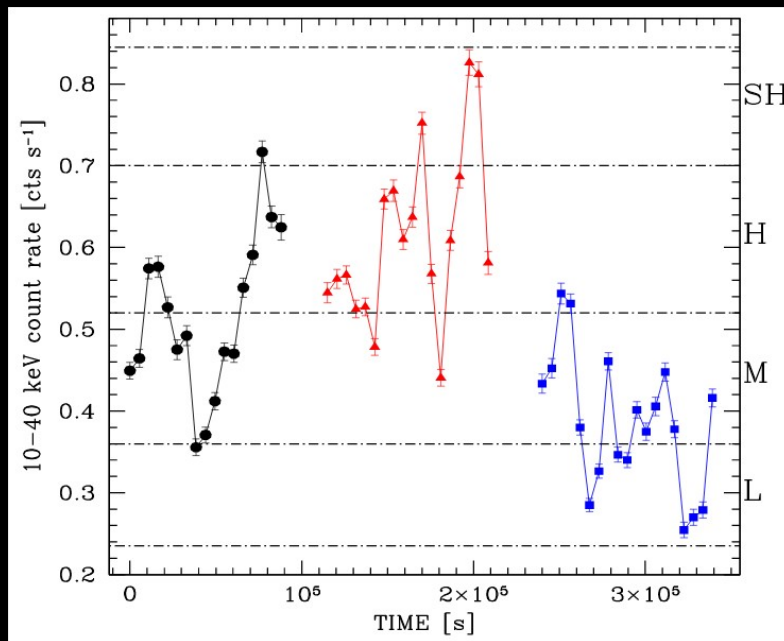
Previous studies revealed the extreme absorbing column density of $N_{\text{H}} \sim 4 \times 10^{24} \text{ cm}^{-2}$ in the source. It completely blocks the primary nuclear emission below 8-10 keV and the nucleus can only be directly seen in higher energy ranges ($>10 \text{ keV}$).

Introduction

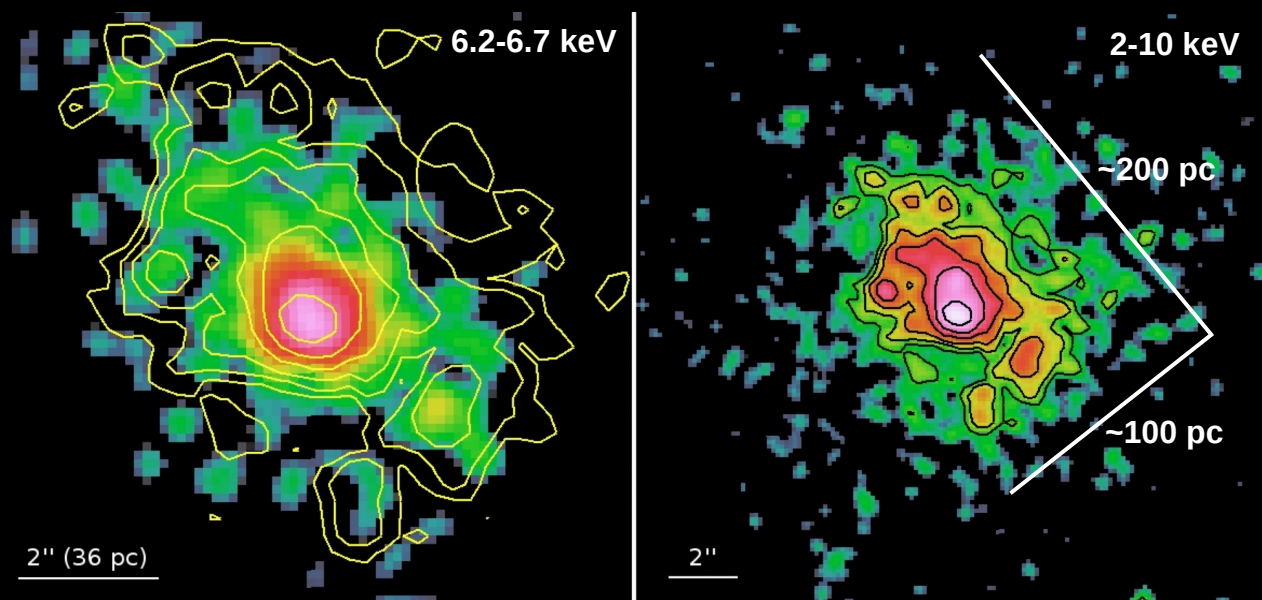


NuSTAR observations confirmed the very variable intrinsic continuum of the source and a constant emission below 10 keV.

Puccetti+14



Introduction

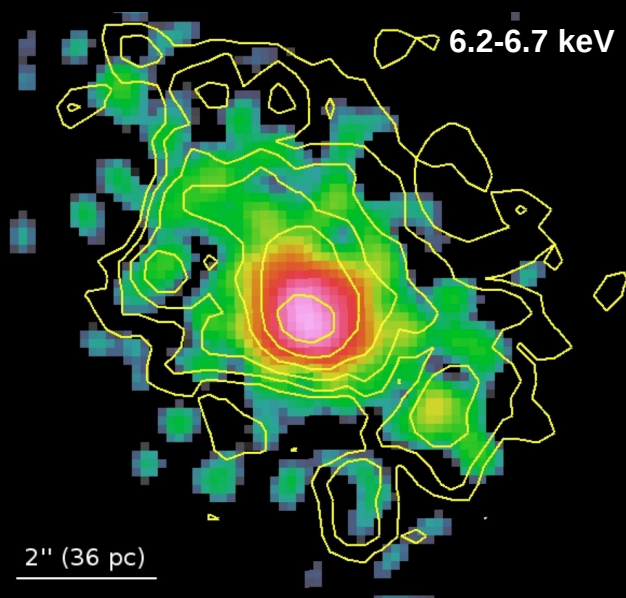


Marinucci+12

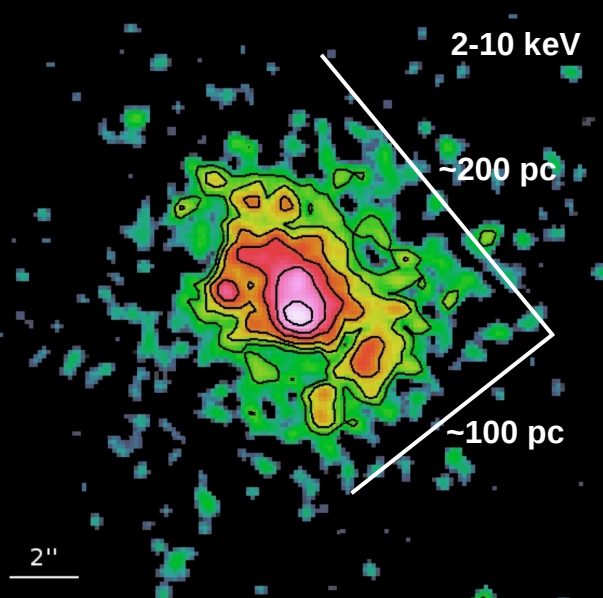
Past imaging analysis with Chandra (~ 230 ks) revealed that the Iron $K\alpha$ and the associated Compton reflection continuum are spatially extended on scales of hundreds of parsecs.

Comparing spectra taken with different instruments (and different extraction regions) on a time scale of ten years, the reprocessed emission is found constant within 4%.

Introduction



Marinucci+12



Past imaging analysis with Chandra (~ 230 ks) revealed that the Iron $K\alpha$ and the associated Compton reflection continuum are spatially extended on scales of hundreds of parsecs.

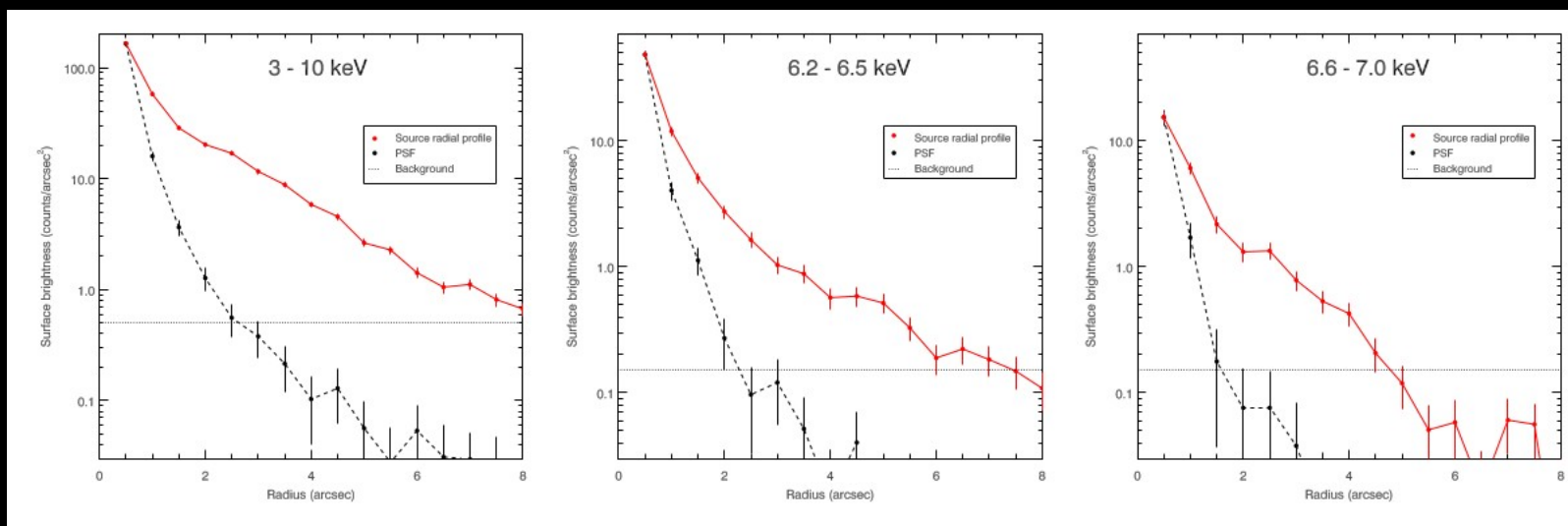
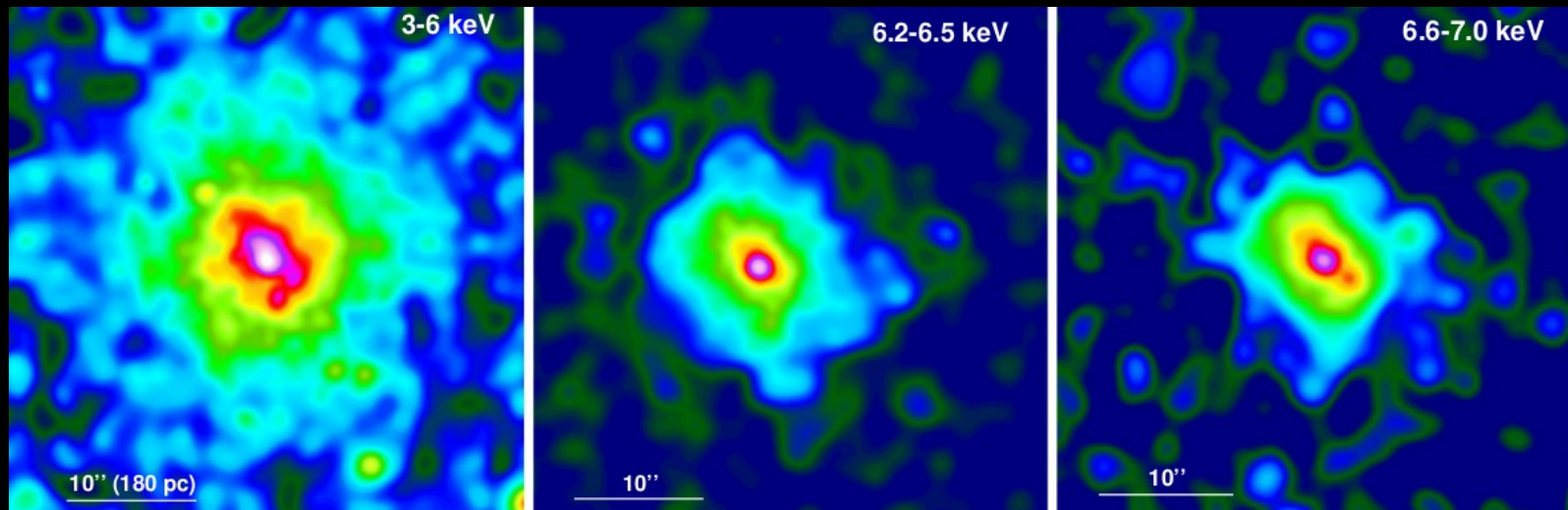
Comparing spectra taken with different instruments (and different extraction regions) on a time scale of ten years, the reprocessed emission is found constant within 4%.

| Obs. ID | Date | Exp. Time (ks) | HETG |
|---------|------------|----------------|------|
| 864 | 2000-01-27 | 49.7 | X |
| 4899 | 2004-05-28 | 78.6 | ✓ |
| 4900 | 2004-05-29 | 95.8 | ✓ |
| 14985 | 2013-04-20 | 68.7 | X |
| 14984 | 2013-04-25 | 130.5 | X |

Table 1. Observation log for the *Chandra* ACIS-S observations of NGC 4945.

Imaging analysis

When images in different energy bands are extracted from the combined event file, 420 ks long, a clump of ionized iron emerges on the south-east direction, 2.2" (~40 pc) from the nucleus.

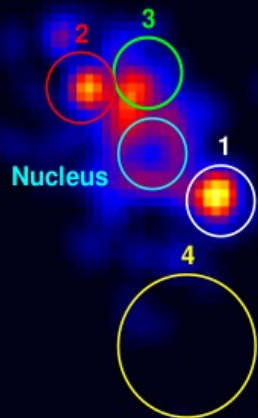


Marinucci et al., submitted

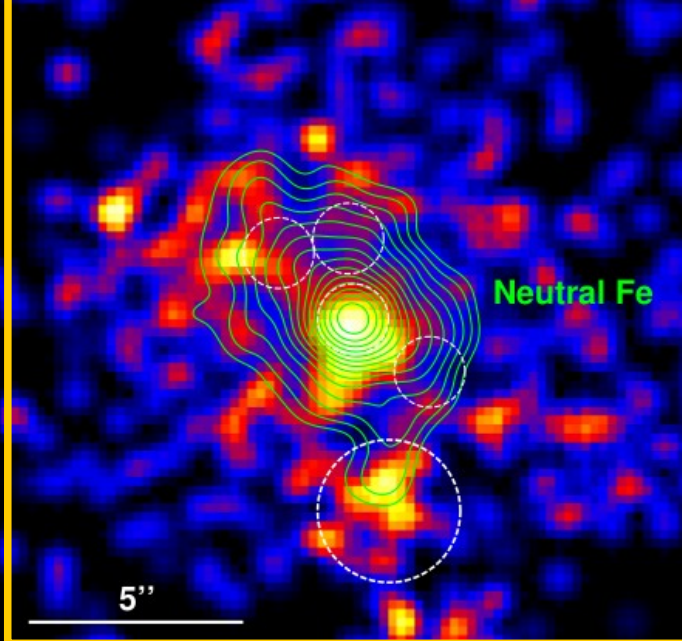
Imaging analysis

The ratios between the three images are proxies of the EW of the lines and can be helpful in choosing extraction regions.

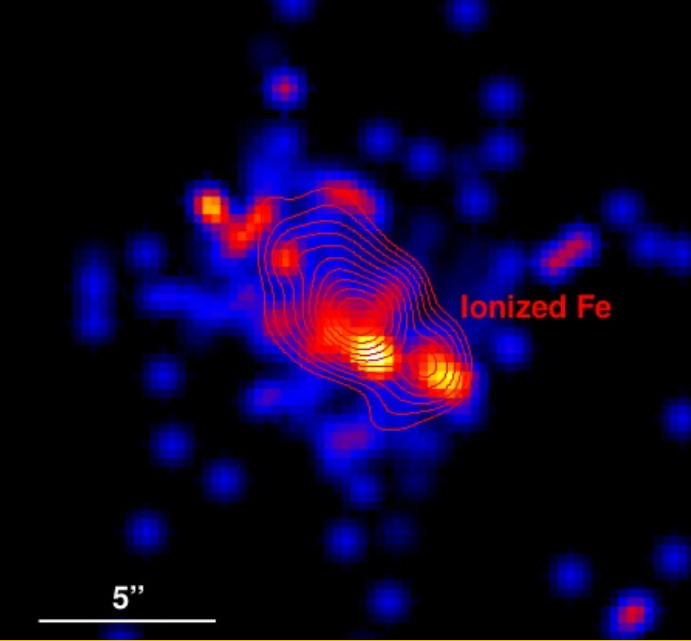
Ratio Ionized Fe/ Neutral Fe



Ratio Neutral Fe/ Continuum



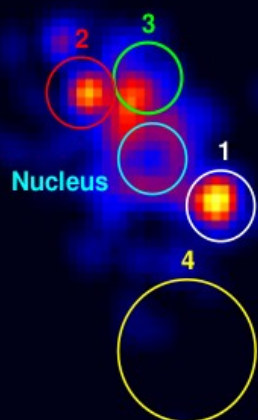
Ratio Ionized Fe/ Continuum



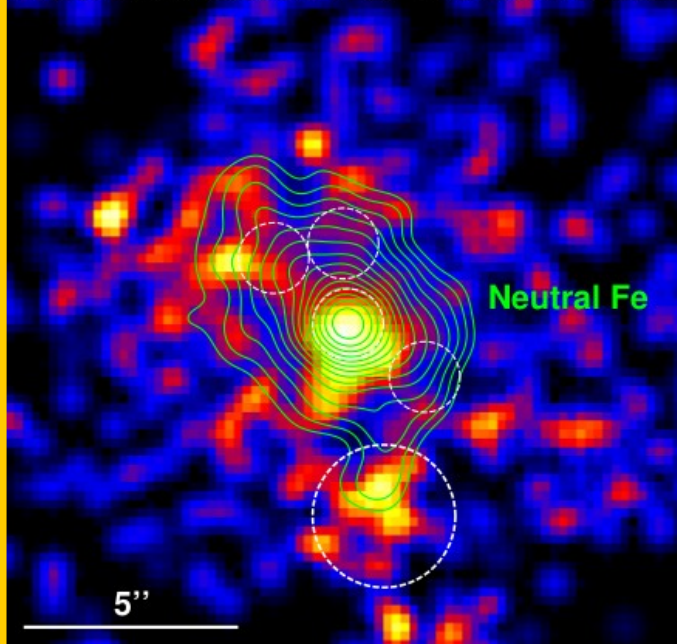
Imaging analysis

The ratios between the three images are proxies of the EW of the lines and can be helpful in choosing extraction regions.

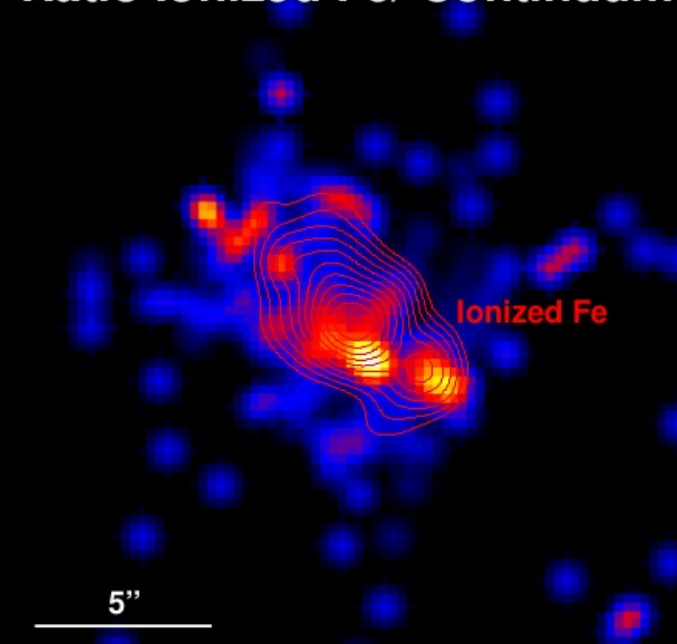
Ratio Ionized Fe/ Neutral Fe



Ratio Neutral Fe/ Continuum



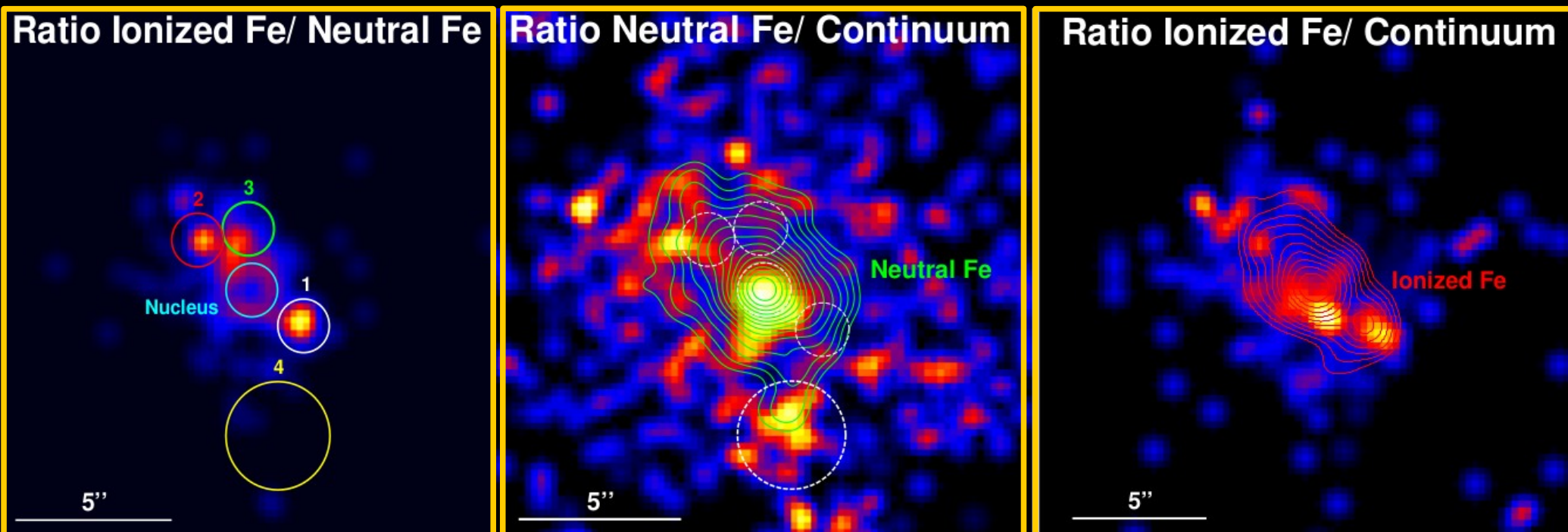
Ratio Ionized Fe/ Continuum



| Obs. ID | 3–10 keV Counts | | | | | |
|---------|-------------------|-----|-----|-----|---------|------|
| | Extraction region | | | | | |
| | 1 | 2 | 3 | 4 | Nucleus | |
| 864 | } | 361 | 303 | 460 | 148 | 359 |
| 14984 | | | | | | 1029 |
| 14985 | | | | | | 588 |
| 4899 | } | 116 | 138 | 163 | 46 | 370 |
| 4900 | | | | | | 424 |

Imaging analysis

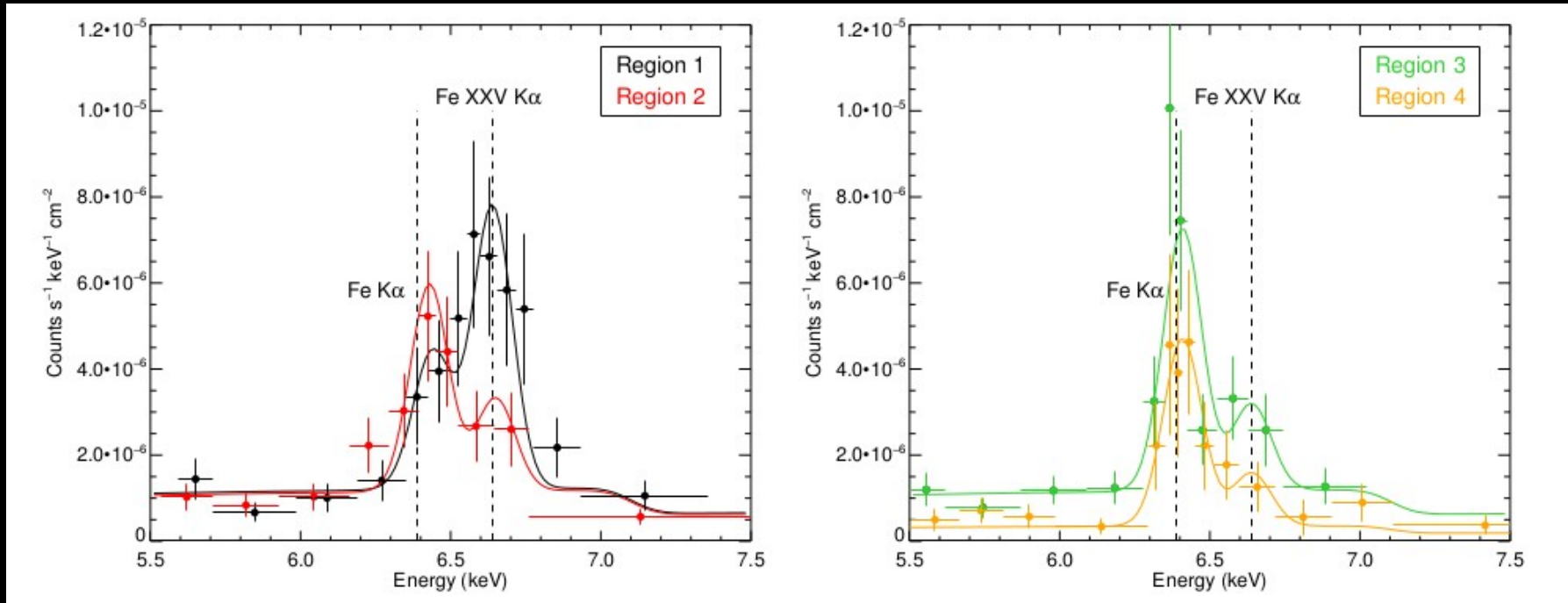
The ratios between the three images are proxies of the EW of the lines and can be helpful in choosing extraction regions.



| Obs. ID | 3–10 keV Counts | | | | | |
|---------|-------------------|-----|-----|-----|---------|------|
| | Extraction region | | | | Nucleus | |
| | 1 | 2 | 3 | 4 | | |
| 864 | } | 361 | 303 | 460 | 148 | 359 |
| 14984 | | | | | | 1029 |
| 14985 | | | | | | 588 |
| 4899 | } | 116 | 138 | 163 | 46 | 370 |
| 4900 | | | | | | 424 |

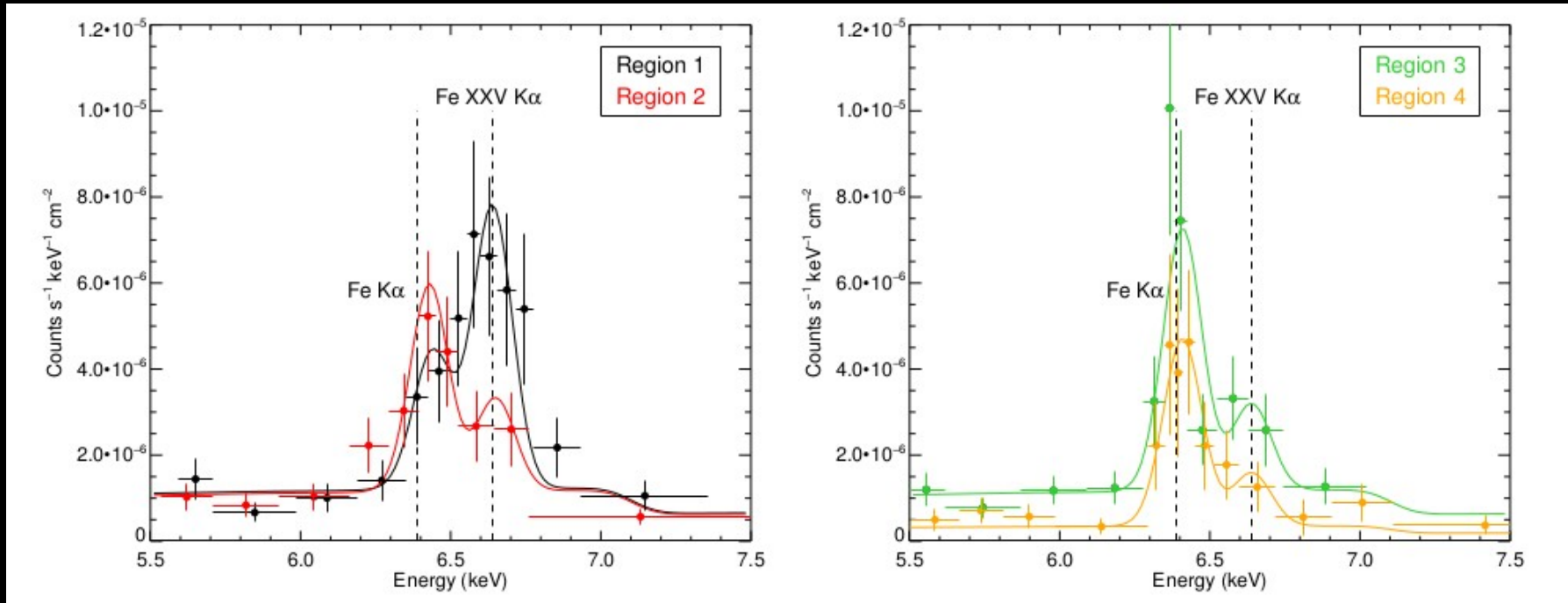
The unresolved, nuclear emission confirms to remain constant throughout the 13 years of monitoring. The Equivalent Width of the neutral Fe K α emission line is 2.7 ± 0.5 keV.

Spectral analysis



| Parameter | Reg. 1 | Reg. 2 | Reg. 3 | Reg. 4 |
|------------------------------------|------------------------|------------------------|------------------------|------------------------|
| N_{pexrav} | 0.40 ± 0.03 | 0.39 ± 0.03 | 0.37 ± 0.08 | 0.12 ± 0.02 |
| Fe Kα | | | | |
| Energy | 6.44 ± 0.05 | 6.43 ± 0.03 | 6.40 ± 0.03 | $6.40^{+0.02}_{-0.03}$ |
| Flux | 0.05 ± 0.02 | 0.08 ± 0.02 | 0.09 ± 0.03 | 0.07 ± 0.02 |
| EW | $0.45^{+0.30}_{-0.20}$ | $0.65^{+0.30}_{-0.25}$ | $0.75^{+0.40}_{-0.25}$ | $2.15^{+1.30}_{-0.85}$ |
| Fe xxv Kα | | | | |
| Energy | $6.65^{+0.03}_{-0.04}$ | 6.66 ± 0.07 | 6.65 ± 0.06 | 6.60 ± 0.10 |
| Flux | 0.11 ± 0.03 | 0.04 ± 0.02 | 0.03 ± 0.02 | 0.02 ± 0.01 |
| EW | 0.90 ± 0.30 | 0.30 ± 0.25 | 0.35 ± 0.30 | $0.60^{+0.70}_{-0.45}$ |
| $F_{3-10 \text{ keV}}$ | 0.80 ± 0.07 | 0.75 ± 0.08 | 0.85 ± 0.08 | 0.28 ± 0.05 |
| C/d.o.f. | 37/51 | 65/40 | 28/38 | 26/31 |

Spectral analysis



| Parameter | Reg. 1 | Reg. 2 | Reg. 3 | Reg. 4 |
|------------------------------------|------------------------|------------------------|------------------------|------------------------|
| N_{pexrav} | 0.40 ± 0.03 | 0.39 ± 0.03 | 0.37 ± 0.08 | 0.12 ± 0.02 |
| Fe Kα | | | | |
| Energy | 6.44 ± 0.05 | 6.43 ± 0.03 | 6.40 ± 0.03 | $6.40^{+0.02}_{-0.03}$ |
| Flux | 0.05 ± 0.02 | 0.08 ± 0.02 | 0.09 ± 0.03 | 0.07 ± 0.02 |
| EW | $0.45^{+0.30}_{-0.20}$ | $0.65^{+0.30}_{-0.25}$ | $0.75^{+0.40}_{-0.25}$ | $2.15^{+1.30}_{-0.85}$ |
| Fe xxv Kα | | | | |
| Energy | $6.65^{+0.03}_{-0.04}$ | 6.66 ± 0.07 | 6.65 ± 0.06 | 6.60 ± 0.10 |
| Flux | 0.11 ± 0.03 | 0.04 ± 0.02 | 0.03 ± 0.02 | 0.02 ± 0.01 |
| EW | 0.90 ± 0.30 | 0.30 ± 0.25 | 0.35 ± 0.30 | $0.60^{+0.70}_{-0.45}$ |
| $F_{3-10 \text{ keV}}$ | 0.80 ± 0.07 | 0.75 ± 0.08 | 0.85 ± 0.08 | 0.28 ± 0.05 |
| C/d.o.f. | 37/51 | 65/40 | 28/38 | 26/31 |

The variable Fe K α EW

The Fe K α EW, depends on the Fe abundance (Matt et al, 1997),
on the angle θ between the polar direction and the line of sight
(Matt et al., 1991; George & Fabian, 1991)
and on the column density of the illuminated material
(Yaqoob et al. 2010, Matt 2002).

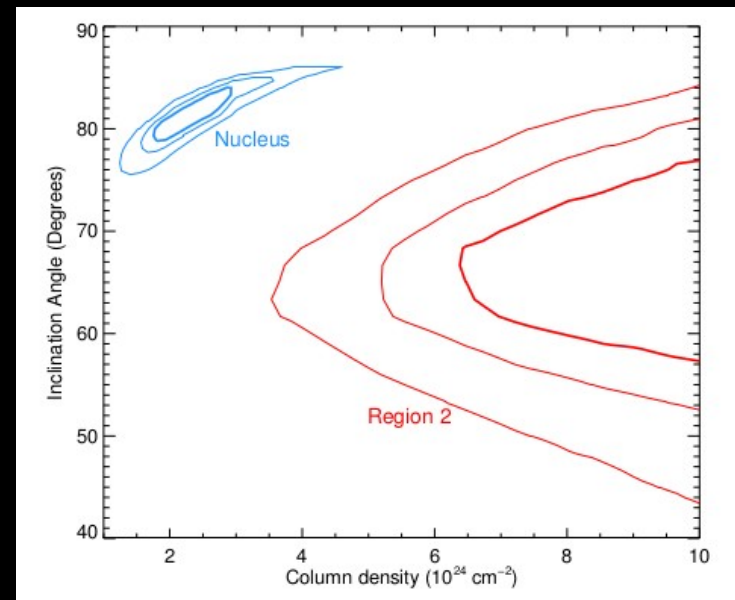
We therefore used different models to retrieve the observed EWs of the Fe Ka in the
nuclear region (2.7 ± 0.5 keV) and in region 2 (0.65 ± 0.30 keV).

Pexmon

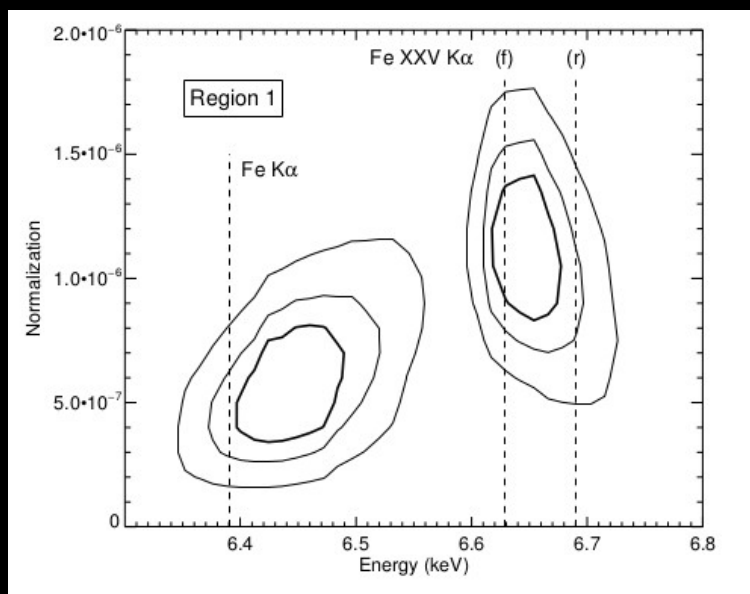
$$A_{\text{fe}}(\text{Nucleus}) = 3.2 \pm 0.4$$

$$A_{\text{fe}}(\text{Region 2}) = 0.8 \pm 0.5$$

MYtorus



The Fe XXV K α clump



The energy centroid of the Fe xxv K α , even though consistent with the resonant line at the 90% confidence level, suggests the predominance of the forbidden line within the triplet.

We can use these results to provide estimates on the gas parameters, such as its column density, the Fe abundance and the ionization state.

With the CLOUDY code we are able to model the spectrum from region 1 in terms of a self-consistent photoionization model and retrieve the best-fit parameters :

$$\log U = 2.2 \pm 0.3$$

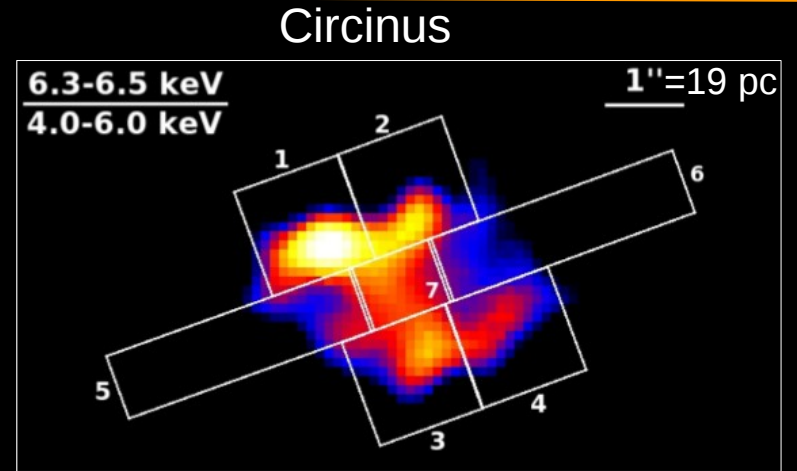
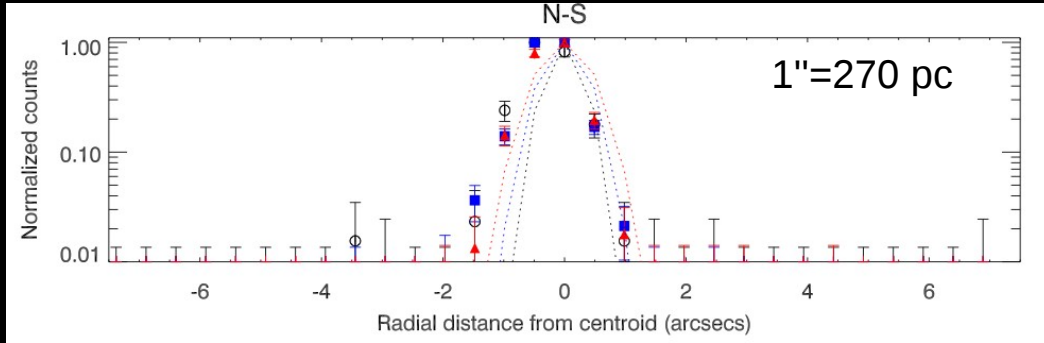
$$\log N_{\text{H}} > 23.5$$

$$A_{\text{Fe}} > 3$$

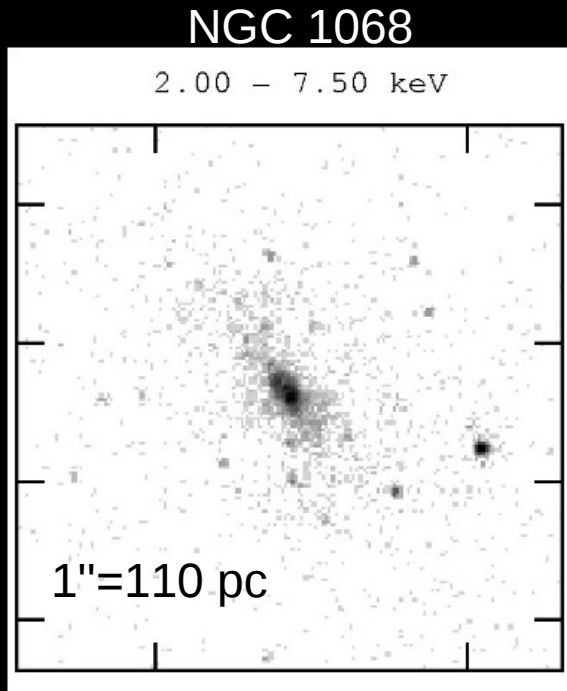
Using the inferred ionization parameter, the SED and L_{2-10} of NGC 4945, at a distance $d=40$ pc the clump has a density $n_{\text{cl}} = 10^2 \text{ cm}^{-3}$.

The Chandra view of nearby CT sources

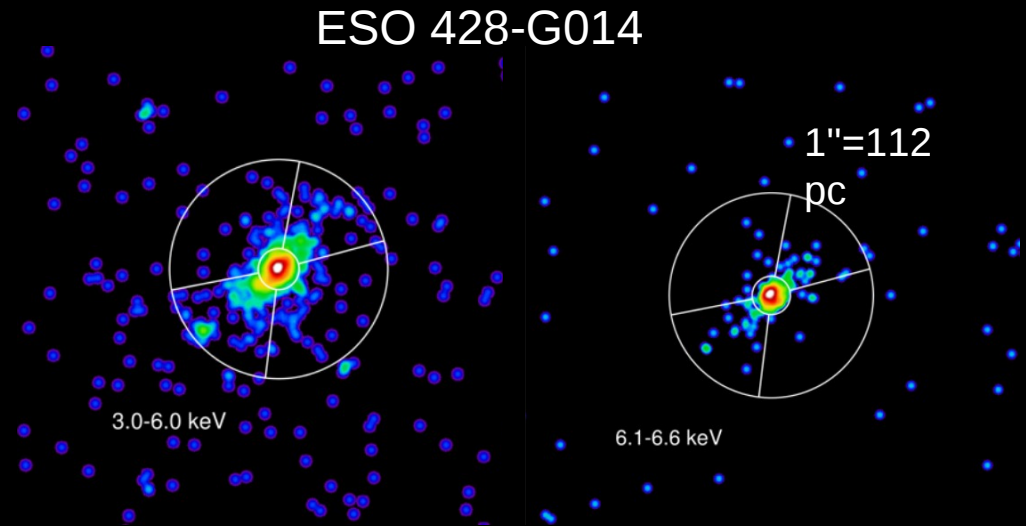
Guainazzi+12



Marinucci+13



Young+01



Fabbiano+17

Conclusions

The additional 200 ks of data on NGC 4945 allowed us to study the extended Iron $K\alpha$ emission and associated reflection continuum with much greater detail:

- the equivalent width of the Iron $K\alpha$ line is found to be spatially variable
- a highly ionized Iron emission in a very confined region, about 40 pc distant from the nucleus, has been detected and spectrally characterised

Our findings support a physical environment around the nucleus which is not homogeneously distributed: the gas responsible for the reprocessing of the nuclear radiation is clumpy and extended around the central region, on scales of hundreds of parsecs.